



TITLE:

# Oxidative Dissolution of Tungsten Metal in NaCO under Ar–O–CO Atmosphere

AUTHOR(S):

Yasuda, Kouji; Nozaki, Fumiyasu; Uehata, Ryotaro; Hagiwara, Rika

---

CITATION:

Yasuda, Kouji ...[et al]. Oxidative Dissolution of Tungsten Metal in NaCO under Ar–O–CO Atmosphere. Journal of The Electrochemical Society 2020, 167(13): 131501.

ISSUE DATE:

2020-09

URL:

<http://hdl.handle.net/2433/255260>

RIGHT:

This is the Accepted Manuscript version of an article accepted for publication in Journal of The Electrochemical Society. IOP Publishing Ltd is not responsible for any errors or omissions in this version of the manuscript or any version derived from it. The Version of Record is available online at <https://doi.org/10.1149/1945-7111/abb4ae>; This is not the published version. Please cite only the published version.; この論文は出版社版ではありません。引用の際には出版社版をご確認ください。

1 **Research Paper submitted to Journal of the Electrochemical Society**

2

3 **Title: Oxidative Dissolution of Tungsten Metal in Na<sub>2</sub>CO<sub>3</sub> under Ar–O<sub>2</sub>–CO<sub>2</sub> atmosphere**

4 Author Names:

5 Kouji YASUDA,<sup>1,2,3, \*, z</sup> Fumiyasu NOZAKI,<sup>1</sup> Ryotaro UEHATA,<sup>1</sup> and Rika HAGIWARA,<sup>1, \*</sup>

6

7 Affiliation(s):

8 <sup>1</sup> Department of Fundamental Energy Science, Graduate School of Energy Science, Kyoto  
9 University, Yoshida-honmachi, Sakyo-ku, Kyoto 606-8501, Japan.

10 <sup>2</sup> Agency for Health, Safety and Environment, Kyoto University, Yoshida-honmachi, Sakyo-ku,  
11 Kyoto 606-8501, Japan.

12 <sup>3</sup> Present address: Department of Materials Science and Engineering, Graduate School of  
13 Engineering, Kyoto University, Yoshida-honmachi, Sakyo-ku, Kyoto 606-8501, Japan.

14

15

16 \* Electrochemistry Society Active Member

17 <sup>z</sup>Corresponding Author:

18 E-mail Address: [yasuda.kouji.3v@kyoto-u.ac.jp](mailto:yasuda.kouji.3v@kyoto-u.ac.jp) (K. Yasuda)

19

20 ORCID

21 Kouji Yasuda: <https://orcid.org/0000-0001-5656-5359>

22 Rika Hagiwara: <https://orcid.org/0000-0002-7234-3980>

23

24 **Abstract**

25 A novel process for the recycling of tungsten from hard tool scraps using carbonate molten salts  
26 is proposed. As a fundamental study, the oxidative dissolution of tungsten metal into molten  $\text{Na}_2\text{CO}_3$   
27 under  $\text{Ar-O}_2$  and  $\text{Ar-O}_2\text{-CO}_2$  atmospheres was investigated at 1173 K. The results of the oxidative  
28 dissolution experiments and the detection of CO gas evolution by infrared spectroscopy revealed the  
29 existence of multiple oxidation mechanisms by peroxide/superoxide ions and carbonate ions. The  
30 feasibility of each oxidant was discussed by calculating potential- $p_{\text{CO}_2}$  diagrams in molten  $\text{Na}_2\text{CO}_3$   
31 at 1173 K. The relationship between the potential and the reaction was investigated using cyclic  
32 voltammetry and potential- $p_{\text{CO}_2}$  diagrams.

33

34 **Keywords**

35 Tungsten, Molten salts, Carbonate, Recycling

36

## 37 Introduction

38

39 Tungsten is one of the critical metals that demonstrates favorable properties such as high hardness,  
 40 wear resistance, and thermal resistance. Tungsten is processed into special steel (e.g., high-speed steel  
 41 and heat-resistant steel, cemented hard tools (e.g., cutting tools and abrasive tools), and processed  
 42 materials (e.g., plates, wires, and bars) for lighting and electronic components. Cemented hard tools  
 43 are composed of tungsten carbide (WC) particles and cobalt metal binders. The application includes  
 44 a wide range of industrial fields such as automobiles, aircrafts, and civil engineering. In 2017, the  
 45 application of cemented hard tools accounted for approximately 80% in Japan.<sup>1</sup>

46 China dominates the supply of the tungsten resource with *ca.* 60% reserves and 80% mine  
 47 production.<sup>2</sup> In certain circumstances like mine accidents, the resource supply could be unstable.  
 48 Consequently, it is important to ensure the resource security and recycle tungsten scraps to use as  
 49 secondary resources. However, the domestic recycling rate in Japan was only 11.6% in 2017.<sup>1</sup> Thus,  
 50 the recycling of the cemented hard tool scraps is urgently required.

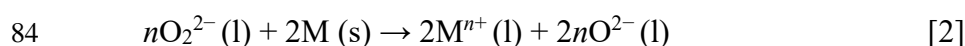
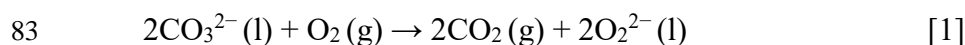
51 There are three major recycling methods for cemented hard tool scraps that are commercially  
 52 used globally: zinc alloying method, thermal oxidation method, and molten nitrate method.<sup>3</sup> In the  
 53 zinc alloying method, WC particles are recovered by crashing the scraps after the alloying/dealloying  
 54 reaction of metallic Zn and Co. In the thermal oxidation method, scraps are calcined in air at high  
 55 temperature; then, the surface oxide layer is leached in the alkali solutions, which is a treatment called  
 56 peeling. Since oxidation is limited to the surface layer, the necessity of repeated calcination and  
 57 leaching is a drawback owing to the high process cost. In the molten nitrate method, which is the  
 58 most modern method, the scraps are oxidatively dissolved in molten NaNO<sub>3</sub> at 700–900 °C using the  
 59 oxidizing power of nitrate.<sup>3–5</sup> The resultant Na<sub>2</sub>WO<sub>4</sub> is then purified by wet processing. Even though  
 60 the fast reaction rate is an advantage, this method has several disadvantages due to the emission of  
 61 NO<sub>x</sub> gas and the difficulty in controlling the intensive exothermic reaction. Other molten salt methods  
 62 using sulfates or hydroxides have been reported as recycling processes for tungsten materials.<sup>6–15</sup>

63 This study proposes a novel molten carbonate method for recycling tungsten from cemented hard  
 64 tool scraps. Figure 1 depicts a flowchart of the molten carbonate method. The scraps are oxidatively  
 65 dissolved in molten Na<sub>2</sub>CO<sub>3</sub> under an Ar–O<sub>2</sub>–CO<sub>2</sub> atmosphere. The produced Na<sub>2</sub>WO<sub>4</sub> is treated  
 66 using the same wet processing and hydrogen reduction of WO<sub>3</sub> as the molten nitrate method. Single  
 67 Na<sub>2</sub>CO<sub>3</sub> was chosen from various single and mixed carbonates because it allows the use of solid-  
 68 liquid separation and ion exchange in the downstream process for sodium systems, which have been  
 69 already established in industrial scale **for the molten nitrate method.**<sup>3–5</sup> One of the advantages of this  
 70 method is that it does not require repeated peeling since the use of molten carbonate enables the

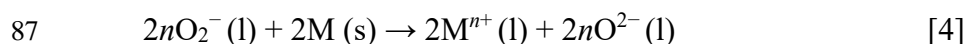
71 dissolution of the formed oxide into the molten salt. Another advantage is its environmentally  
 72 friendliness due to the avoidance of NO<sub>x</sub> gas emissions. In addition, the reaction is easily controlled  
 73 by the partial pressures of O<sub>2</sub> and CO<sub>2</sub>, which are the parameters for oxidation and basicity,  
 74 respectively. However, a disadvantage is that the reaction speed of the oxidation reaction for the  
 75 proposed method is slower than that for the molten nitrate method.

76 Since oxidative dissolution reaction is a corrosion reaction, several methods were used to analyze  
 77 the corrosion of metals in molten carbonates. The corrosion behavior in molten Li<sub>2</sub>CO<sub>3</sub>–K<sub>2</sub>CO<sub>3</sub> was  
 78 investigated for application in molten carbonate fuel cells (MCFC), and analyzed for Fe, Ni, Cr, and  
 79 stainless steel using thermogravimetry<sup>16–21</sup> and for Ni, Fe–Cr alloy, and Ni–Fe alloy using  
 80 electrochemical methods.<sup>22–25</sup> The oxidation and corrosion of these metals occur by peroxide (O<sub>2</sub><sup>2-</sup>)  
 81 and superoxide (O<sub>2</sub><sup>-</sup>) ions formed by the chemical dissolution of O<sub>2</sub> gas into the melt.<sup>26</sup>

82



85



88

89 However, the corrosion behavior of less common metals including tungsten in molten carbonates is  
 90 scarce, and the reaction of W metal and WC to molten carbonates is only reported in vacuum at 1123  
 91 K<sup>27</sup> and in air at 1073–1273 K.<sup>28</sup> These reports only demonstrated the products without any analytical  
 92 results for the reaction mechanism. In particular, the dependence on partial pressure of CO<sub>2</sub>, which is  
 93 the controlling factor for the basicity of molten carbonates, has not been investigated.

94 Since the elucidation of the reaction mechanism is crucial to achieve the proposed recycling  
 95 process, this study was aimed at providing a knowledge on the thermodynamics and kinetics of the  
 96 oxidative dissolution of cemented hard tools into molten Na<sub>2</sub>CO<sub>3</sub> by selecting W metal as the model  
 97 sample. First, the quantity of W metal oxidatively dissolved in molten Na<sub>2</sub>CO<sub>3</sub> under an Ar–O<sub>2</sub>–CO<sub>2</sub>  
 98 atmosphere at 1173 K was measured, and the reaction mechanism was discussed using the  
 99 dependence on CO<sub>2</sub> partial pressure, reaction in an Ar–CO<sub>2</sub> atmosphere, and gas analysis. Second,  
 100 the oxidative dissolution of W metal and WC was analyzed using thermodynamic calculations. Last,  
 101 several factors of oxidative dissolution such as oxidant species and corrosion potential were  
 102 investigated cyclic voltammetry.

103

104

105

\*\*\* Fig. 1 \*\*\*

106

107

## 108 Experimental

109

### 110 *Oxidative dissolution in Na<sub>2</sub>CO<sub>3</sub> molten salt.*

111 Figure 2 illustrates the experimental setup used for the oxidative dissolution experiment.  
 112 Powdery Na<sub>2</sub>CO<sub>3</sub> (Fuji Film Wako Pure Chemical Corp., >99.8%) and W plate (Nilaco Corp., 99.95%,  
 113 *ca.* 10 × 10 × 0.3 mm) were placed in an alumina crucible (Nikkato Corp., SSA-S, C1, 30 mL, height  
 114 24 mm) and dried overnight in a vacuum at 453 K. The Na<sub>2</sub>CO<sub>3</sub> powder was weighed such that the  
 115 depth of molten salt was 4 mm, 6 mm, or 9 mm. The three crucibles with melts at different depths  
 116 were set on an Au base plate (Nilaco Corp., thickness 0.1 mm) to prevent the upset and tilting, and  
 117 were inserted into an airtight vessel composed of a stainless-steel flange and a quartz reaction tube  
 118 (outer diameter: 46 mm, inner diameter: 42 mm, length: 400 mm). The temperature of the reaction  
 119 tube set in a horizontal furnace was raised from room temperature to 1173 K at a rate of 5 K min<sup>-1</sup>  
 120 and maintained for a reaction time of 0–2.5 h, where the melting temperature of Na<sub>2</sub>CO<sub>3</sub> is 1131 K.  
 121 After the reaction, the temperature was lowered to room temperature at a rate of 5 K min<sup>-1</sup>. Herein,  
 122 the reaction time indicates the duration for which the furnace was maintained at 1173 K. Thus, at 0 h,  
 123 the reaction was conducted only by raising the temperature to 1173 K then immediately lowering the  
 124 temperature without holding at that temperature. The flow rate of the mixed-gas was controlled by a  
 125 mass flow controller (Horiba STEC Co. Ltd., SEC-E40 or PE-D20). The flow rate was fixed to 50  
 126 mL min<sup>-1</sup> and the partial pressure was controlled by each flow rate; the partial pressure of CO<sub>2</sub> at  
 127 6 × 10<sup>-4</sup> atm was attained at a rate of 0.03 mL min<sup>-1</sup>. The flowing gas was Ar–CO<sub>2</sub> (6 × 10<sup>-4</sup>–0.8 atm)  
 128 during the heating and cooling, then switched to Ar–O<sub>2</sub>–CO<sub>2</sub> (Ar–O<sub>2</sub>: 0.2 atm, CO<sub>2</sub>: 6 × 10<sup>-4</sup>–0.8 atm)  
 129 during the reaction at 1173 K. The partial pressure of CO<sub>2</sub> was kept constant throughout the  
 130 experiment. In the experiment used to investigate the reaction mechanism without the effect of O<sub>2</sub>  
 131 gas, the reaction was conducted in Ar–CO<sub>2</sub> (6 × 10<sup>-4</sup>–0.8 atm). In several experiments, the outlet gas  
 132 from the furnace was sampled into a plastic bag and analyzed using Fourier transform infrared  
 133 spectroscopy (FT-IR, Bruker Corp., ALPHA II).

134 The recovered salts were crushed in a mortar and analyzed by X-ray diffraction (XRD, Rigaku  
 135 Corp., MiniFlex, Cu-K $\alpha$  line, 30 kV, 10 mA). The weight change in the W plate and the amount of W  
 136 dissolved in the molten carbonate determined by inductive coupled plasma-atomic emission  
 137 spectroscopy (ICP-AES, Hitachi Ltd., SPECTRO BLUE) correlated with each other. The dissolved  
 138 thickness of the W plate ( $x_w$ ) was evaluated from the weight of the plate before the reaction ( $w_{W,bef}$ )

139 and the weight loss ( $w_{W,dec}$ ). The evaluation was made under the assumption that the dissolution  
140 reaction only proceeded from the upper surface of the plate.

141  
142 
$$x_w (\mu\text{m}) = 300 \times w_{W,dec} / w_{W,bef} \quad [5]$$

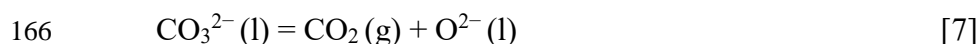
143  
144  
145  
146  
147

\*\*\* Fig. 2 \*\*\*

148 ***Electrochemical analysis in the Na<sub>2</sub>CO<sub>3</sub> molten salt.***

149 Fig. 3 depicts a schematic drawing of the experimental apparatus used in electrochemical  
150 measurements. Na<sub>2</sub>CO<sub>3</sub> (300 g) was charged in an alumina crucible (As One Corp., >99%, outer  
151 diameter: 90 mm, inner diameter: 80 mm, height: 140 mm) and dried under vacuum at 453 K for  
152 more than 12 h to remove the moisture. The crucible was then placed at the bottom of a quartz vessel  
153 in an airtight quartz container in a vertical furnace. The controlled atmosphere was as described above.  
154 The measurement was conducted in Ar–O<sub>2</sub>–CO<sub>2</sub> (Ar–O<sub>2</sub>: 0.2 atm, CO<sub>2</sub>:  $6 \times 10^{-4}$  atm) and Ar–O<sub>2</sub>–  
155 CO<sub>2</sub> (Ar–O<sub>2</sub>: 0.2 atm, CO<sub>2</sub>: 0.8 atm), hereinafter low-CO<sub>2</sub> and high-CO<sub>2</sub> partial pressures, respectively.

156 Electrochemical measurements were performed at 1173 K by a three-electrode method using an  
157 electrochemical measurement system (Hokuto Denko Corp., HZ-7000). The working electrodes were  
158 Au wire (Japan Metal Service, Ltd., 99.99%, diameter: 0.5 mm) and W plate (Nilaco Corp., 10 × 10  
159 × 0.1 mm, 99.95%). Au plate (Japan Metal Service, Ltd., 99.99%, 0.1 mm thick) was used as a counter  
160 electrode. Au wire immersed in the molten salt was used as a quasi-reference electrode. Since the  
161 atmosphere and the molten salt contains O<sub>2</sub> gas and O<sup>2-</sup> ions, respectively, the potential of the quasi-  
162 reference electrode would correspond to the O<sub>2</sub>/O<sup>2-</sup> equilibrium at the given partial pressure of O<sub>2</sub>  
163 gas and the activity of O<sup>2-</sup> ions determined by the partial pressure of CO<sub>2</sub>.



167  
168

The potential of the quasi-reference electrode is discussed in results and discussion.

169  
170  
171  
172

\*\*\* Fig. 3 \*\*\*

173 **Results and Discussion**

174

175 ***Oxidative dissolution and thermodynamic analysis.***

176 After the reaction, white salt and W plate were recovered as shown in the photographs in Fig.  
177 4(a) and (b), respectively, which were the representative reacted samples obtained under the  
178 conditions of 0.2 atm O<sub>2</sub>, 6 × 10<sup>-4</sup> atm CO<sub>2</sub>, and 2.5 h. As shown in the XRD spectrum of the salt in  
179 Fig. 4(c), the diffraction peaks of Na<sub>2</sub>WO<sub>4</sub> and Na<sub>2</sub>CO<sub>3</sub> are confirmed, thus verifying the oxidative  
180 dissolution of the W plate as the W(VI) compound. The appearances and XRD patterns of the sample  
181 after the reaction were similar in all experimental conditions, despite changing the CO<sub>2</sub> partial  
182 pressure and reaction time.

183

184

185

\*\*\* Fig. 4 \*\*\*

186

187

188 Fig. 5 shows the dissolved thickness of the W plate in molten Na<sub>2</sub>CO<sub>3</sub> at 1173 K under the Ar-  
189 O<sub>2</sub>-CO<sub>2</sub> (Ar-O<sub>2</sub>: 0.2 atm, CO<sub>2</sub>: 6×10<sup>-4</sup> atm) atmosphere against the reaction time for each melt depth.  
190 The dissolved thickness is larger at smaller melt depths. The dissolution rate determined from the  
191 slope between the reaction time of 0 and 2.5 h is 23.1, 9.8, and 6.8 μm h<sup>-1</sup> at 4, 6, and 9 mm of the  
192 melt depth, respectively. The dependency of the reaction rate on the depth of the melt suggests that  
193 the rate determining step of the reaction is the diffusion between the gas-liquid interface at the melt  
194 surface and the solid-liquid interface at the surface of the W plate.

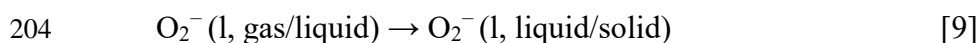
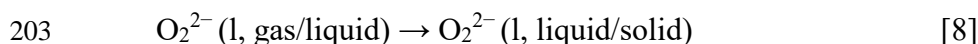
195 The corrosion and oxidative dissolution of the metals in molten carbonates are generally  
196 associated with four elementary steps.<sup>26</sup> Based on the reported mechanisms, the oxidative dissolution  
197 of W metal in this study consists of the following steps:

198

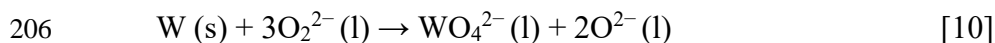
199 (1) Formation of O<sub>2</sub><sup>2-</sup>/O<sub>2</sub><sup>-</sup> ions by the chemical dissolution of O<sub>2</sub> gas at the gas-liquid interface



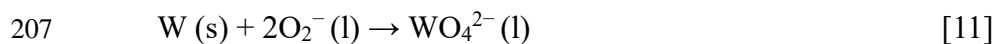
202 (2) Diffusion of O<sub>2</sub><sup>2-</sup>/O<sub>2</sub><sup>-</sup> ions from the gas-liquid interface to the solid-liquid interface



205 (3) Formation of WO<sub>4</sub><sup>2-</sup> ions by the oxidation of W metal







208 (4) Diffusion of  $WO_4^{2-}$  ions from the solid-liquid interface to the bulk melt



210

211 The existence of  $O_2^{2-}/O_2^-$  ions at high partial pressure of  $CO_2$  has been intensively reported in MCFC  
212 researches.<sup>29-42</sup> Their high stability at low partial pressure was also experimentally confirmed.<sup>43,44</sup>  
213 According to the report by Andersen,<sup>43</sup> when the  $O_2-O_2^- - O_2^{2-}-O_2^-$  equilibria were attained for  
214 various carbonate molten salts of Li, Na, and/or K by holding in  $O_2$  (1 atm) after adding 3 mol%  $O_2^-$   
215 ions, a large amount of the added  $O_2^-$  ions reacted with  $O_2$  gas to form  $O_2^{2-}/O_2^-$  ions at the low partial  
216 pressure of  $CO_2$  (the estimated order of  $10^{-4}$  or  $10^{-3}$  atm) by the formed gas in  $CO_3^{2-}$  dissociation. Of  
217 these four elementary steps, steps (2) and (4) correspond to diffusion. Here, the diffusion rate for the  
218  $WO_4^{2-}$  ions in (4) is determined by the thickness of diffusion layer rather than by the melt depth. In  
219 addition, the solubility of the  $WO_4^{2-}$  ions is very high as the  $Na_2CO_3-Na_2W_2O_7$  system shows liquid  
220 state for the entire composition at 1173 K.<sup>45</sup> Therefore, the diffusion of  $O_2^{2-}$  and  $O_2^-$  ions from the  
221 gas-liquid to the solid-liquid interface (step (2)) is the rate-determining step. The dissolution reaction  
222 at (3) is fast enough to keep the ion concentration at the surface of the W plate constant, and the rapid  
223 reaction rate is attained by a higher concentration gradient at a smaller melt depth and a diffusion  
224 distance of  $O_2^{2-}/O_2^-$  oxidants.

225 In Fig. 5, the dissolution of the reaction at 0 h for each melt depth occurs at *ca.* 10  $\mu\text{m}$ . Since  $O_2$   
226 gas was not supplied during the reaction at 0 h, this dissolution occurs in another oxidation mechanism  
227 except in the case of  $O_2^{2-}/O_2^-$  oxidants. The most probable oxidants are  $CO_3^{2-}$  ions at this stage.

228

229

230

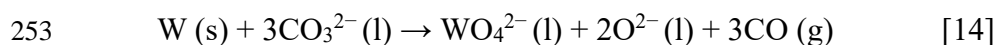
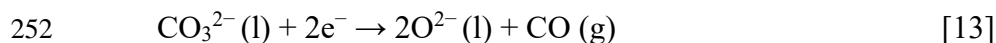
\*\*\* Fig. 5 \*\*\*

231

232

233 The confirmation that  $CO_3^{2-}$  ions also function as oxidants was carried by three types of the  
234 oxidative dissolution experiment in the  $Ar-CO_2$  atmosphere without  $O_2$  gas to observe the  
235 characteristic of  $CO_3^{2-}$  oxidants. First is the occurrence of dissolution without  $O_2$  gas. The appearance  
236 and XRD pattern of the recovered salt and W plate after the reaction were similar regardless the  
237 existence of  $O_2$  gas. The dissolved thickness of the W plate at the 6-mm melt depth for 2.5 h at each  
238  $CO_2$  partial pressure is shown in Fig. 6(a), and a dissolved thickness of approximately 25  $\mu\text{m}$  is  
239 observed even without  $O_2^{2-}/O_2^-$  oxidants. Second is an oxidative dissolution at different melt depths  
240 in the  $Ar-CO_2$  (0.8 atm) atmosphere. The circle and triangle in Fig. 6(a) show the dissolved thickness

241 for 6 and 9 mm of the melt depth, respectively. The identical dissolved thickness agrees with the  
242 characteristic of the  $\text{CO}_3^{2-}$  ions that they exist abundantly in the neighboring region of the molten  
243 salt/W plate interface, which do not require diffusion from the gas/liquid interface. Third experiment  
244 involved IR spectroscopy of the outlet gas. The IR measurement was conducted only for the oxidative  
245 dissolution experiment in the Ar– $\text{CO}_2$  atmosphere without  $\text{O}_2$  gas so that the combustion of CO gas  
246 by the  $\text{O}_2$  component gas to form  $\text{CO}_2$  gas should be avoided. Fig. 6(b) shows the IR spectrum of the  
247 exhaust gas for the oxidative dissolution experiment of tungsten under Ar– $\text{CO}_2$  (0.2 atm) atmosphere  
248 in molten  $\text{Na}_2\text{CO}_3$  at 1173 K. In addition to the component  $\text{CO}_2$  gas, a sharp peak ascribed to the CO  
249 gas is detected which is the byproduct of  $\text{CO}_3^{2-}$  oxidants. These three experiments clearly confirmed  
250 that the  $\text{CO}_3^{2-}$  ions function as an oxidant for the W metal. The representative reaction is as follows:



254  
255 Studies on corrosion protection for MCFC applications have confirmed that the oxidation responsible  
256 for metal corrosion in molten carbonate occurs by  $\text{O}_2^{2-}/\text{O}^{2-}$  ions.<sup>26</sup> Here, it should be noted that this  
257 study confirmed that  $\text{CO}_3^{2-}$  ions also function as oxidants.

260 \*\*\* Fig. 6 \*\*\*

261  
262  
263 Since the oxidizing ability of  $\text{CO}_3^{2-}$  ions was experimentally verified, its thermodynamic aspect  
264 was investigated by drawing a potential– $p_{\text{CO}_2}$  diagram by referring to a previous report by Cassir *et*  
265 *al.*<sup>46</sup> where  $p_{\text{CO}_2}$  is the partial pressure of  $\text{CO}_2$  gas. The diagram draws the equilibrium conditions  
266 and stable region of the related species, where the electrode potential and logarithm of partial pressure  
267 of  $\text{CO}_2$  were the vertical and horizontal axes, respectively.<sup>47</sup> The standard Gibbs energy of formation  
268 ( $\Delta G^\circ_f$ ) for the compounds at 1173 K used for the potential– $p_{\text{CO}_2}$  diagram is summarized in Table  
269 1.<sup>48,49</sup> The standard Gibbs energy of formation of ionic species are defined by selecting the standard  
270 ion and standard potential as follows: the  $\text{O}^{2-} (\text{l})$  ion is selected as the standard ion and its standard  
271 state is the virtual state of the pure  $\text{Na}_2\text{O} (\text{l})$  in  $\text{Na}_2\text{CO}_3 (\text{l})$ . The standard potential is settled for the  
272 equilibrium potential for  $\text{O}_2 (\text{g}, 1 \text{ atm})/\text{O}^{2-} (\text{l}, a = 1)$ .

273



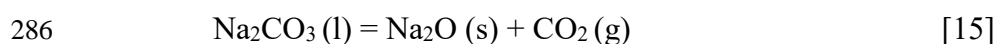
275

276 The standard Gibbs energy of formation of ionic species at 1173 K determined by the above definition  
 277 is listed in Table 2.<sup>48,49</sup> Here, the values for  $O_2^{2-}(l)$  and  $O_2^-(l)$  were calculated under the assumption  
 278 that the reported molar fraction of  $O^{2-}:O_2^{2-}:0.5O_2^- = 51:39:10$  mol% at 1200 K remains applicable at  
 279 1173 K; the aforementioned values were attained at the equilibrium with  $O_2(1 \text{ atm})$  gas after adding  
 280 3 mol%  $O^{2-}$  ions to the molten  $Na_2CO_3$ .<sup>43</sup>

281 The potential- $p_{CO_2}$  diagram for the molten  $Na_2CO_3$  at 1173 K, which was calculated from the  
 282 reported thermodynamic data, is shown in Fig. 7. The region enclosed by the blue lines corresponds  
 283 to the stable region of the molten  $Na_2CO_3$ . The following reactions determine the various limits:

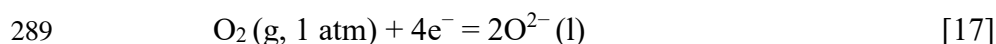
284

285 (1) Precipitation of  $Na_2O(s)$



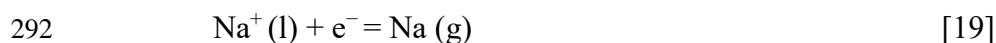
287  $\log p_{CO_2} = -7.11$  [16]

288 (2) Evolution of  $O_2$  gas (anodic limit)



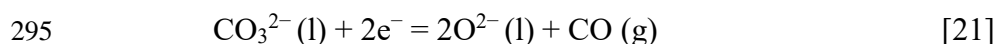
290  $E = 0.116 \log p_{CO_2} + 0.870 \text{ (V)}$  [18]

291 (3) Evolution of Na gas (cathodic limit)



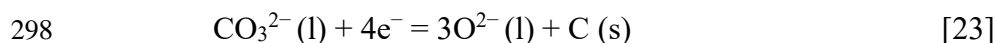
293  $E = -1.273 \text{ (V)}$  [20]

294 (4) Evolution of CO gas (cathodic limit)



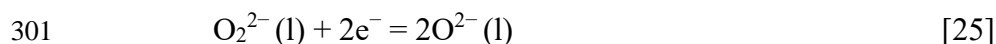
296  $E = 0.233 \log p_{CO_2} - 0.116 \log p_{CO} - 0.066 \text{ (V)}$  [22]

297 (5) Deposition of carbon (cathodic limit)



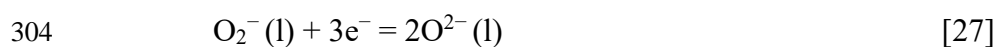
299  $E = 0.175 \log p_{CO_2} - 0.156 \text{ (V)}$  [24]

300 (6) Formation of  $O_2^{2-}$  ions



302  $E = 0.233 \log p_{CO_2} + 0.116 \log a_{O_2^{2-}} - 1.754 \text{ (V)}$  [26]

303 (7) Formation of  $O_2^-$  ions

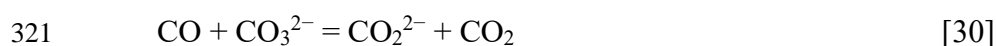


305  $E = 0.155 \log p_{CO_2} + 0.078 \log a_{O_2^-} + 1.262 \text{ (V)}$  [28]

306

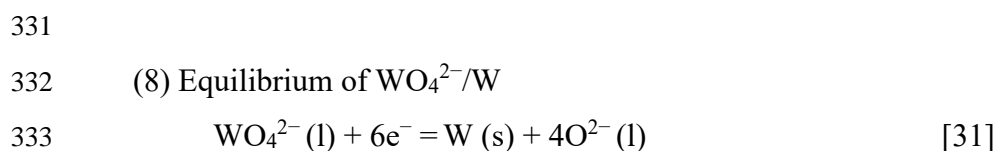
307 where,  $E$  is the potential,  $p_{\text{CO}}$  is the partial pressure of CO gas, and  $a_{\text{O}_2^{2-}}$  and  $a_{\text{O}_2^-}$  are the activities  
308 of  $\text{O}_2^{2-}$  and  $\text{O}_2^-$  ions, respectively.

309 The oxidation power of the two oxidants,  $\text{O}_2^{2-}/\text{O}_2^-$  ions and  $\text{CO}_3^{2-}$  ions, in the molten  $\text{Na}_2\text{CO}_3$  is  
310 depicted in the diagram. The positive redox potentials for reactions (6) and (7) indicate that the  
311  $\text{O}_2^{2-}/\text{O}_2^-$  ions exhibit strong oxidation power. Thus, the  $\text{O}_2^{2-}/\text{O}_2^-$  ions function as oxidants, even for  
312 a species with relatively positive corrosion potential. On the other hand, the oxidation power of the  
313  $\text{CO}_3^{2-}$  ions in reactions (4) and (5) is so weak that only species with more negative corrosion  
314 potentials than those of the  $\text{CO}_3^{2-}/\text{CO}$  and  $\text{CO}_3^{2-}/\text{C}$  equilibriums are oxidized. In other words, both  
315 the  $\text{CO}_3^{2-}$  and  $\text{O}_2^{2-}/\text{O}_2^-$  ions function as oxidants for that kind of negative species. The solubility of  
316 the CO gas physically dissolved into molten carbonates is in the order of  $10^{-7} \text{ mol cm}^{-3} \text{ atm}^{-1}$ .<sup>50,51</sup>  
317 The solubility of the chemical dissolution to form  $\text{CO}_2^{2-}$  ions is larger, in the order of  $10^{-6} \text{ mol cm}^{-3}$   
318  $\text{atm}^{-1}$ .<sup>50,51</sup>

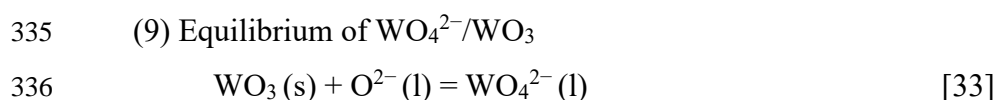


323 The broken lines in Fig. 7 show that the product of the  $\text{CO}_3^{2-}$  oxidant varies with the partial pressure  
324 of CO. When the corrosion potential is substantially negative, the product could be CO gas bubble at  
325 1 atm pressure. At more positive potentials, the partial pressure of CO is lower and the product is  
326 either physically dissolved CO gas or chemically dissolved  $\text{CO}_2^{2-}$  ions.

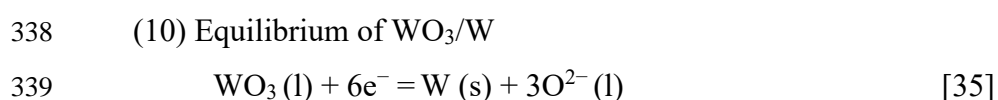
327 The potential- $p_{\text{CO}_2}$  diagram for the W species in molten  $\text{Na}_2\text{CO}_3$  at 1173 K is also drawn in Fig.  
328 7 with red and orange lines for W and WC, respectively. The corresponding reactions and conditions  
329 are shown below. The precipitation of solid  $\text{WO}_3$  is depicted on the far right outside the frame of the  
330 figure.



334 
$$E = 0.155 \log p_{\text{CO}_2} + 0.039 \log a_{\text{WO}_4^{2-}} - 0.332 \quad (\text{V}) \quad [32]$$

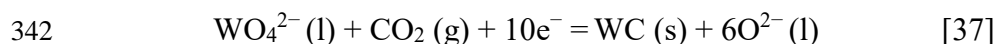


337 
$$\log p_{\text{CO}_2} = -\log a_{\text{WO}_4^{2-}} + 6.786 \quad [34]$$



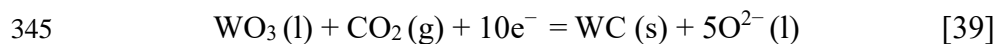
340 
$$E = 0.116 \log p_{\text{CO}_2} - 0.069 \quad (\text{V}) \quad [36]$$

341 (11) Equilibrium of  $\text{WO}_4^{2-}/\text{WC}$



343 
$$E = 0.163 \log p_{\text{CO}_2} + 0.023 \log a_{\text{WO}_4^{2-}} - 0.225 \quad (\text{V}) \quad [38]$$

344 (12) Equilibrium of  $\text{WO}_3/\text{WC}$

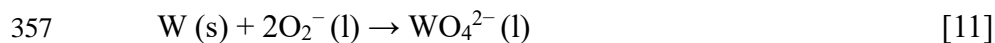
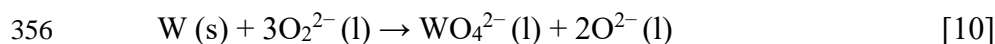


346 
$$E = 0.140 \log p_{\text{CO}_2} - 0.067 \quad (\text{V}) \quad [40]$$

347

348 The red and orange lines indicate the  $\text{WO}_4^{2-}/\text{W}$  and  $\text{WO}_4^{2-}/\text{WC}$  equilibriums for an activity of  $\text{WO}_4^{2-}$   
349 ions ( $a_{\text{WO}_4^{2-}}$ ) of  $10^{-2}$  locate at more negative than the thermodynamic stable region of molten  $\text{Na}_2\text{CO}_3$   
350 at all  $\text{CO}_2$  partial pressures, respectively. These redox potentials clearly indicate that the oxidation of  
351 W and WC by  $\text{CO}_3^{2-}$  ions, which was experimentally confirmed in Fig. 6, is thermodynamically  
352 favorable. Therefore, these results verify that the oxidative dissolution of W metal in molten  $\text{Na}_2\text{CO}_3$   
353 proceeds with both  $\text{O}_2^{2-}/\text{O}_2^-$  and  $\text{CO}_3^{2-}$  ions as oxidants (Fig. 8). One mechanism is (a) oxidation by  
354  $\text{O}_2^{2-}/\text{O}_2^-$  ions produced by the chemical dissolution of  $\text{O}_2$  gas into the molten salt.

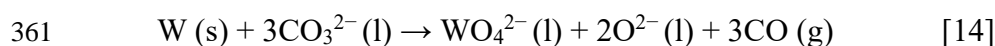
355



358

359 The other mechanism is (b) oxidation by  $\text{CO}_3^{2-}$  ions.

360



362

363

364 \*\*\* Table 1 \*\*\*

365 \*\*\* Table 2 \*\*\*

366 \*\*\* Fig. 7 \*\*\*

367 \*\*\* Fig. 8 \*\*\*

368

369

370 The dependence of the dissolved thickness of the W plates on the partial pressure of  $\text{CO}_2$  for the  
371 molten  $\text{Na}_2\text{CO}_3$  at 1173 K under the Ar- $\text{O}_2$ - $\text{CO}_2$  atmosphere (Ar- $\text{O}_2$ : 0.2 atm) for 2.5 h is shown in  
372 Fig. 9. Although there is a negative correlation between the dissolved thickness and  $\text{CO}_2$  partial

373 pressure at low-CO<sub>2</sub> partial pressures, there is a positive correlation at high-CO<sub>2</sub> partial pressures.  
374 The dependence at low-CO<sub>2</sub> partial pressures occurs by the strong influence of oxidation by O<sub>2</sub><sup>2-</sup>/O<sub>2</sub><sup>-</sup>  
375 ions. The chemical dissolution of O<sub>2</sub> gas into molten Na<sub>2</sub>CO<sub>3</sub> in reactions [1] and [3] is suppressed by  
376 the increase in CO<sub>2</sub> partial pressure. Then, the lowered diffusion flux of O<sub>2</sub><sup>2-</sup>/O<sub>2</sub><sup>-</sup> ions results in a  
377 smaller dissolved thickness of the W plate. On the other hand, the positive correlation in the high-  
378 CO<sub>2</sub> region is due to the oxidation by CO<sub>3</sub><sup>2-</sup> ions, which is facilitated by the low activity of O<sup>2-</sup> ions  
379 at high-CO<sub>2</sub> partial pressures (reaction [14]).

380

381

382

\*\*\* Fig. 9 \*\*\*

383

384

### 385 *Cyclic voltammetry.*

386 The electrochemistry of molten Na<sub>2</sub>CO<sub>3</sub> was investigated by cyclic voltammetry at 1173 K. The  
387 voltammogram at low-CO<sub>2</sub> partial pressure, Ar–O<sub>2</sub>–CO<sub>2</sub> (Ar–O<sub>2</sub>: 0.2 atm, CO<sub>2</sub>: 6×10<sup>-4</sup> atm), was  
388 measured using an Au electrode and is shown in Fig. 10(a). The rest potential is 0 V vs. Au because  
389 the working and quasi-reference electrodes were both made of Au immersed in the molten salt. In the  
390 potential sweep to the negative direction, a small reduction current is observed from the rest potential,  
391 then a large reduction current starts at approximately –0.85 V. The reduction current sharply increases  
392 at –1.7 V. After the reversal of the sweep direction, the oxidation current starts to flow at 0 V and has  
393 a peak at 0.7 V. The potential of the quasi-reference electrode can be calibrated to the value indicated  
394 in the potential–*p*<sub>CO<sub>2</sub></sub> diagram (Fig. 7) under the conditions that the O<sub>2</sub>/O<sup>2-</sup> reaction is  
395 electrochemically reversible and the potential of the reference electrode corresponds to the O<sub>2</sub>/O<sup>2-</sup>  
396 equilibrium at the given partial pressure.

397



$$399 \quad E = 0.116 \log p_{\text{CO}_2} + 0.058 \log p_{\text{O}_2} + 0.870 \quad (\text{V}) \quad [42]$$

400

401 Because the estimated equilibrium potential of the Au quasi-reference electrode is 0.455 V (vs. O<sub>2</sub> (1  
402 atm)/O<sup>2-</sup> (*a* = 1)) at *p*<sub>CO<sub>2</sub></sub> = 6 × 10<sup>-4</sup> atm and *p*<sub>O<sub>2</sub></sub> = 0.2 atm, the calibration enables analysis of the  
403 cyclic voltammogram. Here, the calibration assumption should be noticed that the reversibility for  
404 electrochemical reaction [41] is unknown for low partial pressure of CO<sub>2</sub> although it is well-known  
405 for high partial pressure and the utilization of an Au electrode in 67%CO<sub>2</sub>–33%O<sub>2</sub> gas as a reference

406 electrode has been established. The oxidation at potentials more positive than 0 V indicates the  
 407 evolution of O<sub>2</sub> gas. The small reduction current from 0 V to -0.8 V indicates the reduction of O<sub>2</sub> gas.  
 408 The large reduction current at -0.85 V corresponds to  $p_{\text{CO}} = 10^{-3}$  atm for the reduction of CO<sub>3</sub><sup>2-</sup>  
 409 ions (reaction [21]). At this potential, CO<sub>2</sub><sup>2-</sup> ions are produced because the partial pressure of CO is  
 410 too small for it to be gas bubbles. The large reduction current at -1.7 V corresponds to the evolution  
 411 potential of Na gas (reaction [19] and equation [20]). In summary, the reactions in molten Na<sub>2</sub>CO<sub>3</sub> at  
 412 low-CO<sub>2</sub> partial pressure and at 1173 K are identified as shown by the arrows at the bottom in Fig.  
 413 10(a): (A) O<sub>2</sub> gas evolution at potentials more positive than 0 V, (B) O<sub>2</sub> reduction at potentials more  
 414 negative than 0 V, (C) CO<sub>3</sub><sup>2-</sup> reduction to CO<sub>2</sub><sup>2-</sup> ions, and (D) Na gas evolution. While the strict  
 415 agreement of the potential for (D) Na gas evolution at -1.7 V suggests the validity of the calibration  
 416 or the error within the range of 0.05 V, the reversibility of O<sub>2</sub>/O<sup>2-</sup> redox reaction on an Au electrode  
 417 should be investigated in the future. At this CO<sub>2</sub> partial pressure, the rest potential, i.e. the corrosion  
 418 potential, of the W metal electrode is -0.94 V vs. Au. This potential clearly indicates that the oxidant  
 419 of the W metal is not only O<sub>2</sub><sup>2-</sup>/O<sub>2</sub><sup>-</sup> ions but also CO<sub>3</sub><sup>2-</sup> ions because it is in the potential region of  
 420 (C) CO<sub>3</sub><sup>2-</sup> reduction to CO<sub>2</sub><sup>2-</sup> ions.

421 Cyclic voltammetry was also conducted at high-CO<sub>2</sub> partial pressure, O<sub>2</sub>-CO<sub>2</sub> (O<sub>2</sub>: 0.2, CO<sub>2</sub>: 0.8  
 422 atm). The voltammogram obtained on an Au electrode is indicated in Fig. 10(b). Although the small  
 423 reduction current of approximately -10 mA cm<sup>-2</sup> starting at 0 V is the same as that at low-CO<sub>2</sub>  
 424 pressure, the increase in the reduction current at -1.2 V is smaller. A small anodic current peak is  
 425 observed after the reversal at -1.8 V. Since the equilibrium potential of O<sub>2</sub>/O<sup>2-</sup> at the given  
 426 atmosphere is 0.818 V (vs. O<sub>2</sub> (1 atm)/O<sup>2-</sup> ( $a = 1$ )), the potential region and corresponding reaction  
 427 are analyzed as follows: (A) O<sub>2</sub> gas evolution at potentials more positive than 0 V, (B) O<sub>2</sub> reduction  
 428 at potentials more negative than 0 V, (C) CO<sub>3</sub><sup>2-</sup> reduction to CO<sub>2</sub><sup>2-</sup> ions at  $E < -0.6$  V, and (E) CO<sub>3</sub><sup>2-</sup>  
 429 reduction to C deposition at  $E < -0.9$  V. The existence of an overpotential for the C deposition on the  
 430 Au electrode is suggested since the starting potential is more negative than that by the thermodynamic  
 431 estimation. The rest and corrosion potential of W metal of -1.20 V at high-CO<sub>2</sub> pressure are in the  
 432 potential region of (E) CO<sub>3</sub><sup>2-</sup> reduction to C deposition, and both the O<sub>2</sub><sup>2-</sup>/O<sub>2</sub><sup>-</sup> and CO<sub>3</sub><sup>2-</sup> ions  
 433 thermodynamically function as the oxidants of the W metal.

434

435

436

\*\*\* Fig. 10 \*\*\*

437

438

439

440 ***Characteristics of  $O_2^{2-}/O_2^-$  and  $CO_3^{2-}$  oxidants.***

441 As explained in Fig. 8, the oxidative dissolution of the W metal into molten  $Na_2CO_3$  proceeds in  
 442 two mechanisms. The comparison of the dissolved thickness of the W metal in Ar- $O_2$ - $CO_2$  (Fig. 9)  
 443 and Ar- $CO_2$  (Fig. 6(a)) atmospheres shows that the contribution of  $O_2^{2-}/O_2^-$  ions is almost  
 444 comparable with that of  $CO_3^{2-}$  ions despite the strong oxidizing power, as indicated by the positive  
 445 redox potential in the potential- $p_{CO_2}$  diagram. The reason for the aforementioned observation is the  
 446 solubility in molten  $Na_2CO_3$ . The solubility of the  $O_2^{2-}/O_2^-$  ions at 0.2 atm  $O_2$  partial pressure  
 447 calculated from the report by Appleby and Drunen<sup>50</sup> is in the order of  $10^{-7}$  mol  $cm^{-3}$ . On the other  
 448 hand, the concentration of  $CO_3^{2-}$  ions calculated from the density of  $Na_2CO_3$  ( $1.953$  g  $cm^{-3}$  at 1173  
 449 K)<sup>52</sup> is  $1.84 \times 10^{-2}$  mol  $cm^{-3}$ . A concentration value that is five orders of magnitude is the source of  
 450 the relatively large contribution of  $CO_3^{2-}$  ions despite the small oxidation power.

451 Among the oxidants, an enhanced dissolution rate is expected for the oxidation by  $O_2^{2-}/O_2^-$  ions.  
 452 The increase in the dissolution rate by  $CO_3^{2-}$  oxidants is probably difficult because the concentration  
 453 of  $CO_3^{2-}$  ions in the melt is constant and the rate is independent of  $CO_2$  partial pressure, as shown in  
 454 Fig. 6(a). The increase in the dissolution rate by the  $O_2^{2-}/O_2^-$  oxidant is expected to be possible  
 455 because it depends on the melt depth,  $CO_2$  partial pressure, and concentration of  $O_2^{2-}/O_2^-$  ions. The  
 456 typical improvement is the introduction of  $O_2$  gas into the molten salt to shorten the diffusion distance  
 457 of the  $O_2^{2-}/O_2^-$  ions to the scrap surface.

458

459

460 **Conclusions**

461 The molten carbonate method was proposed as a new recycling process of tungsten contained in  
 462 cemented hard tools. As a fundamental study of this process, W metal was selected as the model  
 463 sample, and the thermodynamics and kinetics for the oxidative dissolution of W metal into molten  
 464  $Na_2CO_3$  at 1173 K were investigated. Oxidative dissolution and the formation of  $Na_2WO_4$  were  
 465 confirmed in the Ar- $O_2$ - $CO_2$  atmosphere at various partial pressures of  $CO_2$ . The dissolution rate in  
 466 the Ar- $O_2$ - $CO_2$  atmosphere was dependent on the  $CO_2$  partial pressure by changing the basicity. The  
 467 dissolution of W metal was also confirmed in the Ar- $CO_2$  atmosphere without  $O_2$  gas, which  
 468 confirmed the ability of  $CO_3^{2-}$  ions to behaved as an oxidant for W metal, as supported by  
 469 thermodynamics using the calculated potential- $p_{CO_2}$  diagram. The results obtained in this study  
 470 verified that the oxidative dissolution of W metal into molten  $Na_2CO_3$  proceeds via two types of  
 471 oxidation mechanisms by  $O_2^{2-}/O_2^-$  ions and  $CO_3^{2-}$  ions.

472



473

474 **Acknowledgments**

475       This study was partly supported by Tokyo Ohka Foundation for the Promotion of Science and  
476 Technology, Japan Oil, Gas and Metals National Corporation (JOGMEC), and Kyoto Education  
477 Foundation for the Promotion of Science and Technology. The authors thank to Prof. T. Nohira at  
478 Institute of Advanced Energy of Kyoto University for ICP-AES measurements.

479 **References**

- 480 1. JOGMEC, *Material Flow of Mineral Resources 2018*, 13. Tungsten (2019).
- 481 2. U.S. Geological Survey, *Mineral Commodity Summaries 2020* (2020).
- 482 3. Y. Yamamoto, K. Sasaya, T. Fudo, A. Nakano, S. Yamanaka, T. Iguchi, F. Sato, and A. Ikegaya,  
 483 PCT International Patent, WO2010/104009 (2010).
- 484 4. T. Ishida, T. Itakura, H. Moriguchi, and A. Ikegawa, *SEI Technical Review*, **181**, 33 (2012).
- 485 5. T. Hayashi, F. Sato, K. Sasaya, and A. Ikegaya, *SEI Technical Review*, **189**, 8 (2016).
- 486 6. F. H. Scott, United Kingdom Patent, GB791925 (1955).
- 487 7. R. Simon, German Patent, DE3144295 (1981).
- 488 8. A. D. Douglass, K. T. Reilly, and J. E. Landmesser, US Patent, US4603043 (1986).
- 489 9. S. N. Bhosale, S. Mookherjee, and R. M. Pardeshi, *High. Temp. Mater. Processes*, **9**, 147  
 490 (1990).
- 491 10. E. Lassner, *Int. J. Refract. Met. Hard Mater.*, **13**, 35 (1995).
- 492 11. M. Lohse, PCT International Patent, WO96/041768 (1996).
- 493 12. K. B. Shedd, Tungsten Recycling in the United States in 2000, U.S. Geological Survey (2005).
- 494 13. M. Morishita, H. Yamamoto, M. Ikebe, H. Yanagida, and T. Ueno, PCT International Patent,  
 495 WO2014/045579 (2014).
- 496 14. T. Itakura, A. Ikegaya, and Y. Yamamoto, Japanese Patent, 6018958 (2016).
- 497 15. T. Oishi, *Kinzoku*, **87**, 771 (2017).
- 498 16. K. N. Lee and D. A. Shores, *J. Electrochem. Soc.*, **137**, 859 (1990).
- 499 17. B. Kim, H. Yoshitake, H. Yokokawa, N. Kamiya, and K. Ota, *Bull. Chem. Soc. Jpn.*, **66**, 1366  
 500 (1993).
- 501 18. B. Kim, H. Yoshitake, N. Kamiya, and K. Ota, in *Proc. Int. Symp. Molten Salt Chemistry and*  
 502 *Technology*, M. L. Saboungi and H. Kojima, Editor, PV 93-9, p.321, The Electrochemical  
 503 Society Proceedings Series, Pennington, NJ (1993).
- 504 19. K. Ota, S. Mitsushima, K. Kato, and N. Kamiya, in *2nd Symp. Molten Carbonate Fuel Cell*  
 505 *Technology*, J. R. Selman, D. A. Shores, H. C. Maru, and I. Uchida, Editors, PV 90-16, p.318,  
 506 The Electrochemical Society Proceedings Series, Pennington, NJ (1990).
- 507 20. K. Ota, K. Toda, T. Kojima, N. Motohira, and N. Kamiya, in *Proc. 10th Int. Symp. Molten*  
 508 *Salts*, R. T. Carlin, S. Deki, M. Matsunaga, D. S. Newman, J. R. Selman, and G. R. Stafford,  
 509 Editors, PV 96-7, p.406, The Electrochemical Society Proceedings Series, Pennington, NJ  
 510 (1996).
- 511 21. M. Yanagita, S. Baba, K. Takimoto, T. Kojima, N. Ohtori, Y. Tamiya, T. Asai, Y. Miyazaki, and  
 512 M. Azuma, *Denki Kagaku (Electrochemistry)*, **64**, 445 (1996).

- 513 22. A. Nishikata and S. Haruyama, *Corrosion*, **42**, 528 (1986).
- 514 23. J. P. T. Vossen, L. Plomp, and J. H. W. de Wit, *J. Electrochem. Soc.*, **141**, 3040 (1994).
- 515 24. J. P. T. Vossen, A. H. H. Janssen, and J. H. W. de Wit, *J. Electrochem. Soc.*, **143**, 58 (1996).
- 516 25. H. Matsuyama, T. Nishina, and I. Uchida, in *Proc. Int. Symp. Molten Salt Chemistry and*  
 517 *Technology*, M. L. Saboungi and H. Kojima, Editor, PV 93-9, p.436, The Electrochemical  
 518 Society Proceedings Series, Pennington, NJ (1993).
- 519 26. Y. Ito, *Yoyuen no Kagaku*, Industrial Publishing & Consulting, Inc., Tokyo (2005).
- 520 27. M. C. Ball, D. S. Brown, D. Page, and R. R. T. Thurman, *Brit. Ceram. Trans. J.*, **66**, 307  
 521 (1967).
- 522 28. F. H. Scott, United Kingdom Patent, GB791925 (1955).
- 523 29. A. J. Appleby and S. Nicholson, *J. Electroanal. Chem. Interfacial Electrochem.*, **53**, 105  
 524 (1974).
- 525 30. A. J. Appleby and S. B. Nicholson, *J. Electroanal. Chem. Interfacial Electrochem.*, **83**, 309  
 526 (1977).
- 527 31. A. J. Appleby and S. B. Nicholson, *J. Electroanal. Chem. Interfacial Electrochem.*, **112**, 71  
 528 (1980).
- 529 32. G. B. Dunks and D. Stelman, *Inorg. Chem.*, **22**, 2168 (1983).
- 530 33. W. M. Vogel, S. W. Smith, and L. J. Bregoli, *J. Electrochem. Soc.*, **130**, 574 (1983).
- 531 34. I. Uchida, T. Nishina, Y. Mugikura, and K. Itaya, *J. Electroanal. Chem.*, **206**, 229 (1986).
- 532 35. I. Uchida, T. Nishina, Y. Mugikura, and K. Itaya, *J. Electroanal. Chem.*, **206**, 241 (1986).
- 533 36. I. Uchida, T. Nishina, Y. Mugikura, and K. Itaya, *J. Electroanal. Chem.*, **209**, 125 (1986).
- 534 37. S. H. Lu and J. R. Selman, *J. Electrochem. Soc.*, **137**, 1125 (1990).
- 535 38. G. L. Lee and J. R. Selman, *Electrochim. Acta*, **38**, 2281 (1993).
- 536 39. P. Tomczyk, H. Sato, K. Yamada, T. Nishina, and I. Uchida, *J. Electroanal. Chem.*, **391**, 125  
 537 (1995).
- 538 40. R. W. Reeve and A. C. C. Tseung, *J. Electroanal. Chem.*, **403**, 69 (1996).
- 539 41. M. Cassir, B. Malinowska, W. Peelen, K. Hemmes, and J. H. W. de Wit, *J. Electroanal. Chem.*,  
 540 **433**, 195 (1997).
- 541 42. T. Itoh, K. Abe, K. Dokko, M. Mohamedi, I. Uchida, and A. Kasuya, *J. Electrochem. Soc.*, **151**,  
 542 A2042 (2004).
- 543 43. B. K. Andersen, *Acta Chem. Scand.*, **A31**, 242 (1977).
- 544 44. G. Moutiers, M. Cassir, and J. Devynck, *J. Electroanal. Chem. Interfacial Electrochem.*, 315,  
 545 **103** (1991).
- 546 45. E. M. Levin, C. R. Robbins, and H. F. McMurdie, *Phase Diagrams for Ceramists 1969*

- 547            *Supplement*, The American Ceramic Society, Columbus, p. 82 (1969).
- 548    46. M. Cassir, G. Moutiers, and J. Devynck, *J. Electrochem. Soc.*, **140**, 3114 (1993).
- 549    47. M. D. Ingram and G. J. Janz, *Electrochim. Acta*, **10**, 783 (1965).
- 550    48. I. Barin, *Thermochemical Data of Pure Substances, 3rd Edition*, VCH, Weinheim (1995).
- 551    49. M. W Chase, *NIST-JANAF Thermochemical Tables, 4th Edition*, American Chemical Society
- 552            and American Institute of Physics for the National Bureau of Standards, New York (1998).
- 553    50. A. J. Appleby and C. V. Druenen, *J. Electrochem. Soc.*, **127**, 1655 (1980).
- 554    51. A. Borucka and A. J. Appleby, *J. Chem. Soc., Farad. Trans. 1: Physical Chemistry in*
- 555            *Condensed Phases*, **73**, 1420 (1977).
- 556    52. A. T. Ward and G. J. Janz, *Electrochim. Acta*, **10**, 849 (1965).
- 557

558 **Figure Captions**

559

560 **Fig. 1** Flowchart of molten carbonate method for recycling of tungsten proposed in this study.

561 **Fig. 2** Schematic drawing of oxidative dissolution experiment of tungsten metal at 1173 K. (A)  
562 Stainless steel lid, (B) SiO<sub>2</sub> reaction tube, (C) alumina tube, (D) electric furnace, (E)  
563 alumina crucible, (F) molten Na<sub>2</sub>CO<sub>3</sub>, (G) W plate, and (H) Au plate.

564 **Fig. 3** Schematic drawing of electrochemical measurement of tungsten metal at 1173 K. (A)  
565 Stainless steel lid, (B) SiO<sub>2</sub> reaction tube, (C) electric furnace, (D) alumina crucible, (E)  
566 molten Na<sub>2</sub>CO<sub>3</sub>, (F) W plate electrode, (G) Au wire electrode, and (H) Au plate electrode.

567 **Fig. 4** Representative appearance of (a) the recovered salt and (b) W plate, and (c) XRD pattern  
568 of the salt after oxidative dissolution experiment of tungsten plate for 2.5 h in molten  
569 Na<sub>2</sub>CO<sub>3</sub> with 6-mm melt depth at 1173 K in Ar–O<sub>2</sub>(0.2 atm)–CO<sub>2</sub>(6 × 10<sup>-4</sup> atm)  
570 atmosphere.

571 **Fig. 5** Dissolved thickness of tungsten plates in molten Na<sub>2</sub>CO<sub>3</sub> at 1173 K in Ar–O<sub>2</sub>(0.2 atm)–  
572 CO<sub>2</sub>(6 × 10<sup>-4</sup> atm) atmosphere.

573 **Fig. 6** (a) Dependence of dissolved thickness of tungsten plates on CO<sub>2</sub> partial pressure in molten  
574 Na<sub>2</sub>CO<sub>3</sub> at 1173 K for 2.5 h. (b) IR spectrum of the exhaust gas of the oxidative dissolution  
575 experiment of tungsten under Ar–CO<sub>2</sub>(0.2 atm) atmosphere in molten Na<sub>2</sub>CO<sub>3</sub> at 1173 K.

576 **Fig. 7** Calculated potential–*p*<sub>CO<sub>2</sub></sub> diagram from the reported thermodynamic data for W species  
577 (Red line) and WC species (Orange line) in molten Na<sub>2</sub>CO<sub>3</sub> at 1173 K from the reported  
578 thermodynamic data.<sup>48,49</sup> (Blue line) Stable region of molten Na<sub>2</sub>CO<sub>3</sub>. The solid and dotted  
579 color lines correspond to equilibriums at the activity of WO<sub>4</sub><sup>2-</sup> ion to be 10<sup>-2</sup> and 10<sup>-4</sup>,  
580 respectively.

581 **Fig. 8** Schematic illustration of the reaction scheme of oxidative dissolution of tungsten metal in  
582 molten Na<sub>2</sub>CO<sub>3</sub> by (a) O<sub>2</sub><sup>2-</sup>/O<sub>2</sub><sup>-</sup> ions and (b) CO<sub>3</sub><sup>2-</sup> ions

583 **Fig. 9** Dependence of dissolution thickness of tungsten plates on CO<sub>2</sub> partial pressure in molten  
584 Na<sub>2</sub>CO<sub>3</sub> at 1173 K in Ar–O<sub>2</sub>(0.2 atm)–CO<sub>2</sub> atmosphere for 2.5 h.

585 **Fig. 10** Cyclic voltammograms for Au wire electrode in (a) Ar–O<sub>2</sub>(0.2 atm)–CO<sub>2</sub>(6 × 10<sup>-4</sup> atm) and  
586 (b) O<sub>2</sub>(0.2 atm)–CO<sub>2</sub>(0.8 atm) in molten Na<sub>2</sub>CO<sub>3</sub> at 1173 K. Scan rate: 0.1 V s<sup>-1</sup>. (A) O<sub>2</sub>  
587 evolution, (B) O<sub>2</sub> reduction, (C) CO<sub>3</sub><sup>2-</sup> reduction, (D) Na gas evolution, and (E) C  
588 deposition.

589

590

591 Table 1 Standard Gibbs energy of formation at 1173 K.<sup>48,49</sup>

592

| Species                             | $\Delta G_f^\circ / \text{kJ mol}^{-1}$ | Reference |
|-------------------------------------|---|-----------|
| Na <sub>2</sub> CO <sub>3</sub> (l) | -809.612                                | [48]      |
| Na <sub>2</sub> O(s)                | -254.073                                | [48]      |
| Na <sub>2</sub> O(l)                | -245.637                                | [48]      |
| CO <sub>2</sub> (g)                 | -396.072                                | [48]      |
| CO(g)                               | -215.458                                | [48]      |
| C(s)                                | 0                                       | [48]      |
| O <sub>2</sub> (g)                  | 0                                       | [48]      |
| Na(g)                               | 0                                       | [48]      |
| W(s)                                | 0                                       | [49]      |
| WC(s)                               | -35.371                                 | [49]      |
| Na <sub>2</sub> WO <sub>4</sub> (l) | -1109.712                               | [49]      |
| WO <sub>3</sub> (s)                 | -543.810                                | [49]      |

593

594

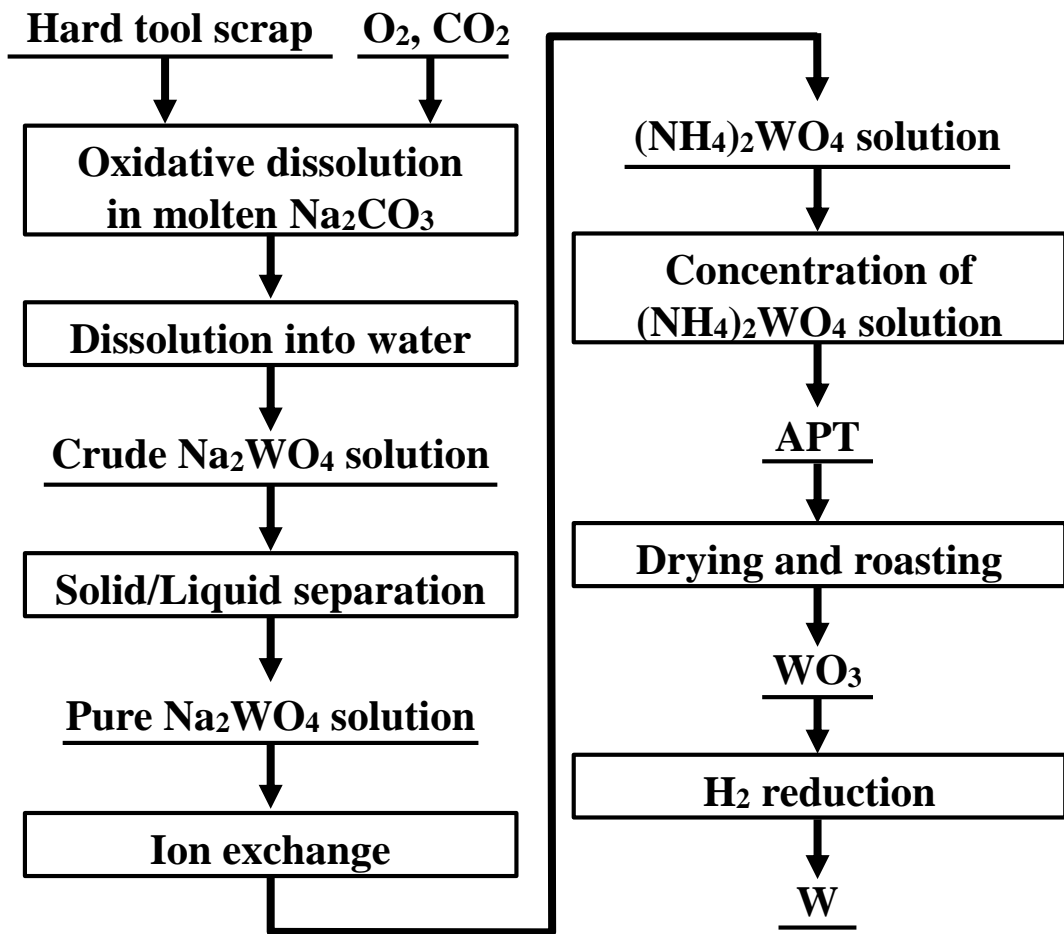
595

596 Table 2 Standard Gibbs energy of formation for ionic species at 1173 K.<sup>48,49</sup>

597

| Species                           | $\Delta G_f^\circ / \text{kJ mol}^{-1}$ |
|-----------------------------------|---|
| O <sup>2-</sup> (l)               | 0                                       |
| CO <sub>3</sub> <sup>2-</sup> (l) | -563.975                                |
| O <sub>2</sub> <sup>2-</sup> (l)  | 2.615 <sup>a</sup>                      |
| O <sub>2</sub> <sup>-</sup> (l)   | 29.497 <sup>a</sup>                     |
| Na <sup>+</sup> (l)               | -122.819                                |
| WO <sub>4</sub> <sup>2-</sup> (l) | -864.075                                |

598 a: Calculated by applying the molar ratio of O<sup>2-</sup>/O<sub>2</sub><sup>2-</sup>/O<sub>2</sub><sup>-</sup> equilibrium in molten Na<sub>2</sub>CO<sub>3</sub> at 1200 K  
 599 to 1173 K.



APT:  
 $(\text{NH}_4)_{10}(\text{H}_2\text{W}_{12}\text{O}_{42}) \cdot 4\text{H}_2\text{O}$

Figure 1 Flowchart of molten carbonate method for recycling of tungsten proposed in this study.

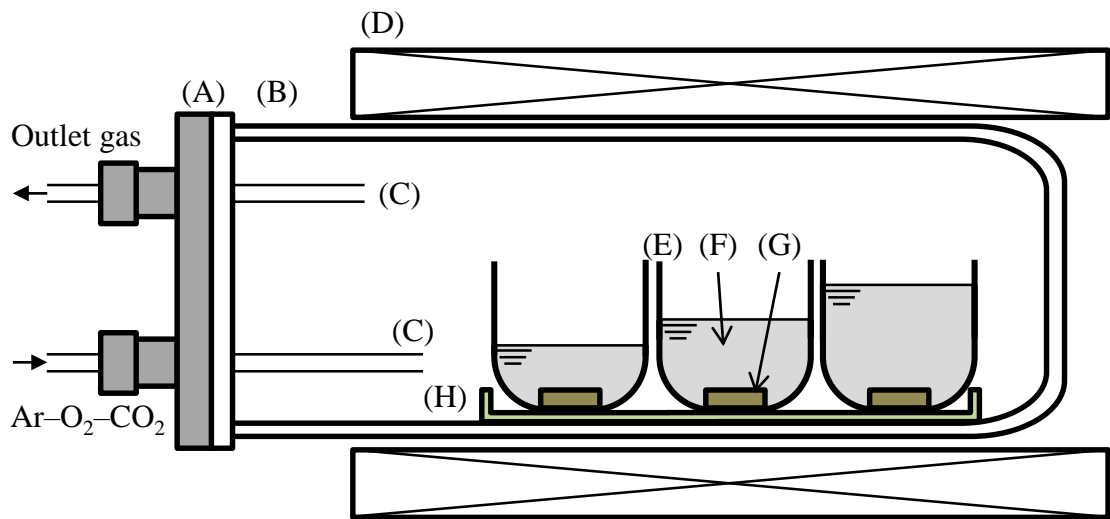


Figure 2 Schematic drawing of oxidative dissolution experiment of tungsten metal at 1173 K. (A) Stainless steel lid, (B) SiO<sub>2</sub> reaction tube, (C) alumina tube, (D) electric furnace, (E) alumina crucible, (F) molten Na<sub>2</sub>CO<sub>3</sub>, (G) W plate, and (H) Au plate.



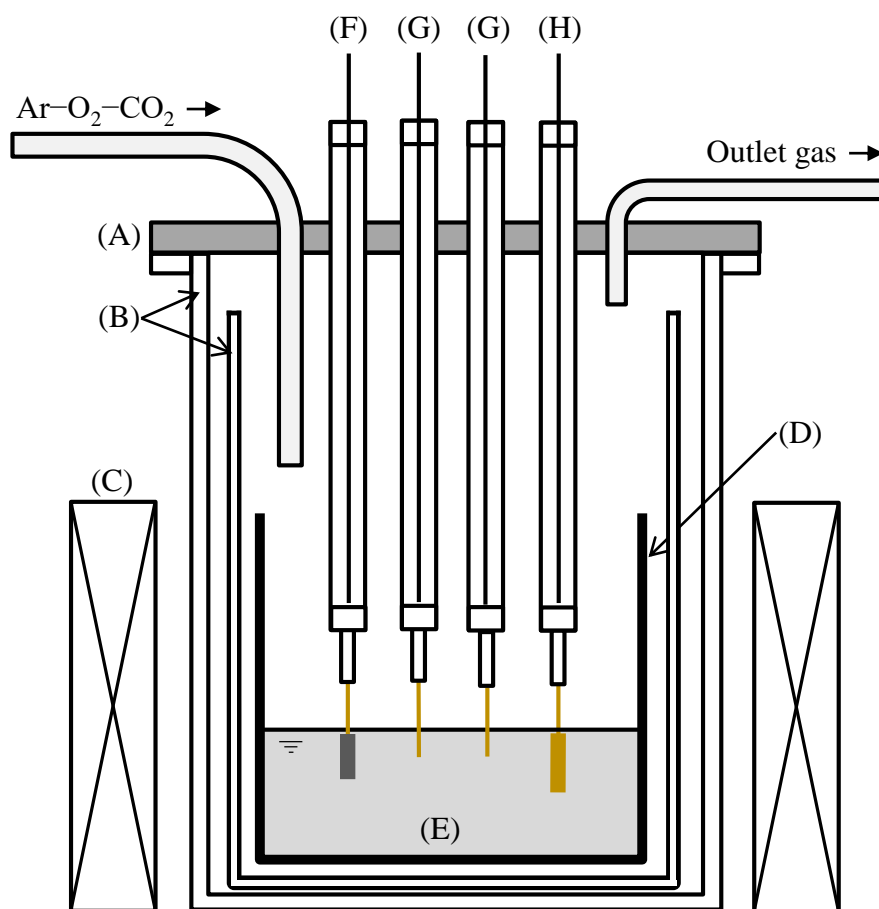


Figure 3 Schematic drawing of electrochemical measurement of tungsten metal at 1173 K. (A) Stainless steel lid, (B) SiO<sub>2</sub> reaction tube, (C) electric furnace, (D) alumina crucible, (E) molten Na<sub>2</sub>CO<sub>3</sub>, (F) W plate electrode, (G) Au wire electrode, and (H) Au plate electrode.

(a) Salt



(b) W plate



(c) XRD (salt)

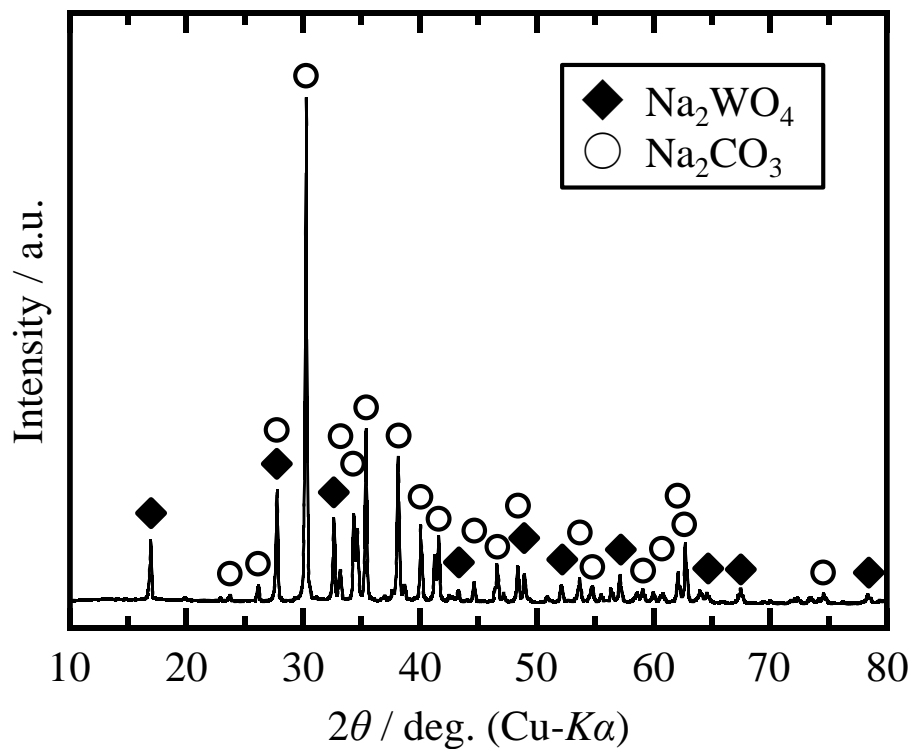


Figure 4 Representative appearance of (a) the recovered salt and (b) W plate, and (c) XRD pattern of the salt after oxidative dissolution experiment of tungsten plate for 2.5 h in molten  $\text{Na}_2\text{CO}_3$  with 6-mm melt depth at 1173 K in  $\text{Ar-O}_2(0.2 \text{ atm})\text{-CO}_2(6 \times 10^{-4} \text{ atm})$  atmosphere.

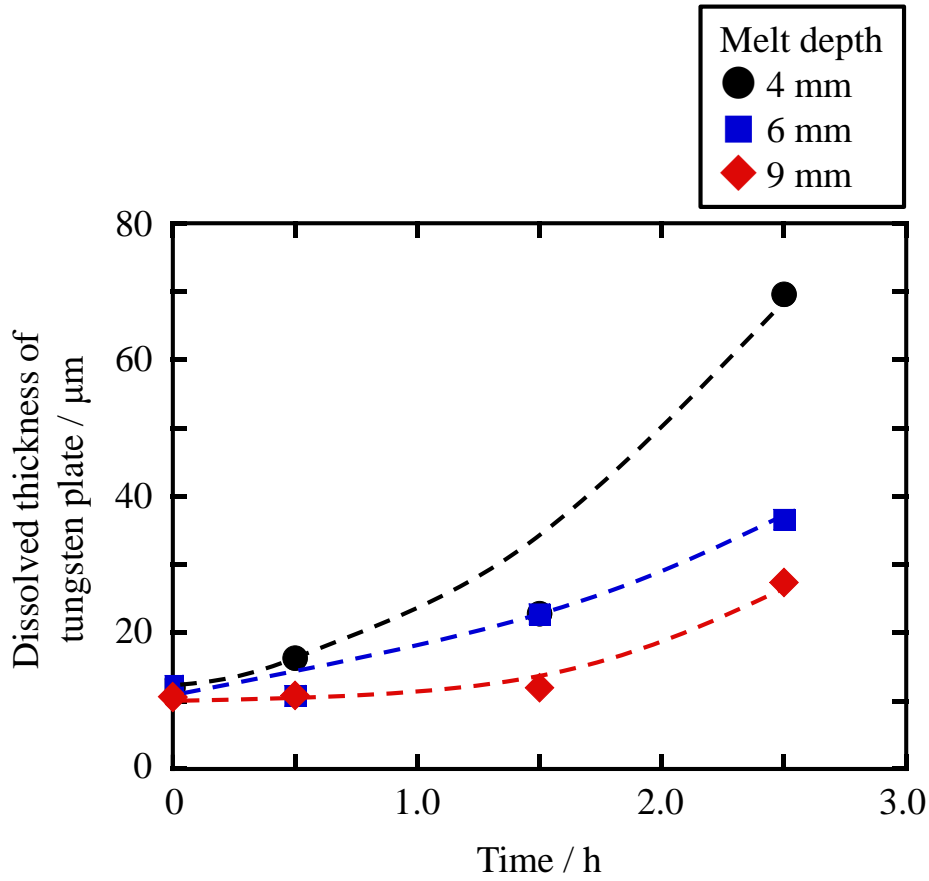


Figure 5 Dissolved thickness of tungsten plates in molten  $\text{Na}_2\text{CO}_3$  at 1173 K in  $\text{Ar-O}_2(0.2 \text{ atm})\text{-CO}_2(6 \times 10^{-4} \text{ atm})$  atmosphere.

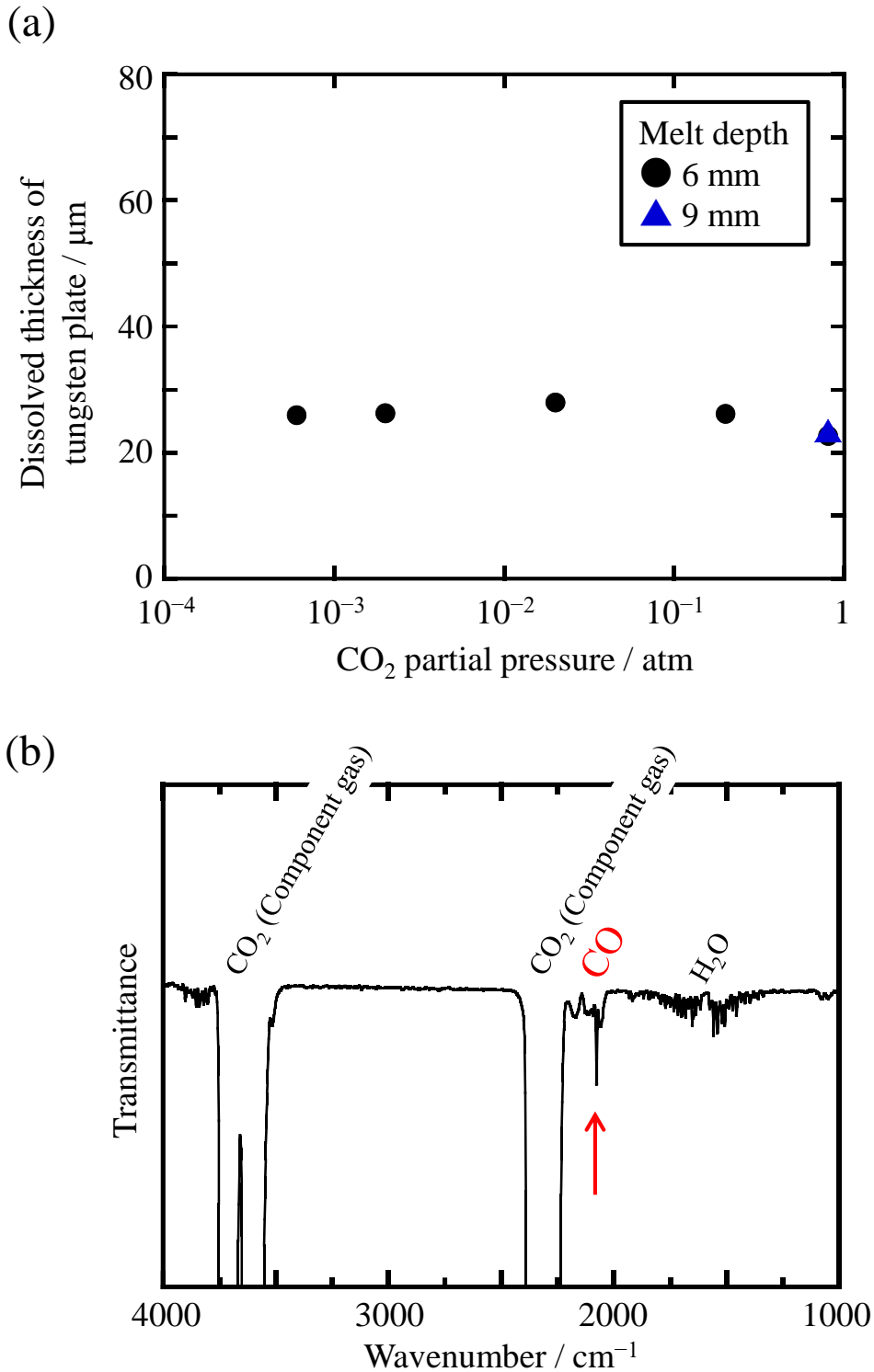


Figure 6 (a) Dependence of dissolved thickness of tungsten plates on CO<sub>2</sub> partial pressure in molten Na<sub>2</sub>CO<sub>3</sub> at 1173 K for 2.5 h. (b) IR spectrum of the exhaust gas of the oxidative dissolution experiment of tungsten under Ar-CO<sub>2</sub>(0.2 atm) atmosphere in molten Na<sub>2</sub>CO<sub>3</sub> at 1173 K.

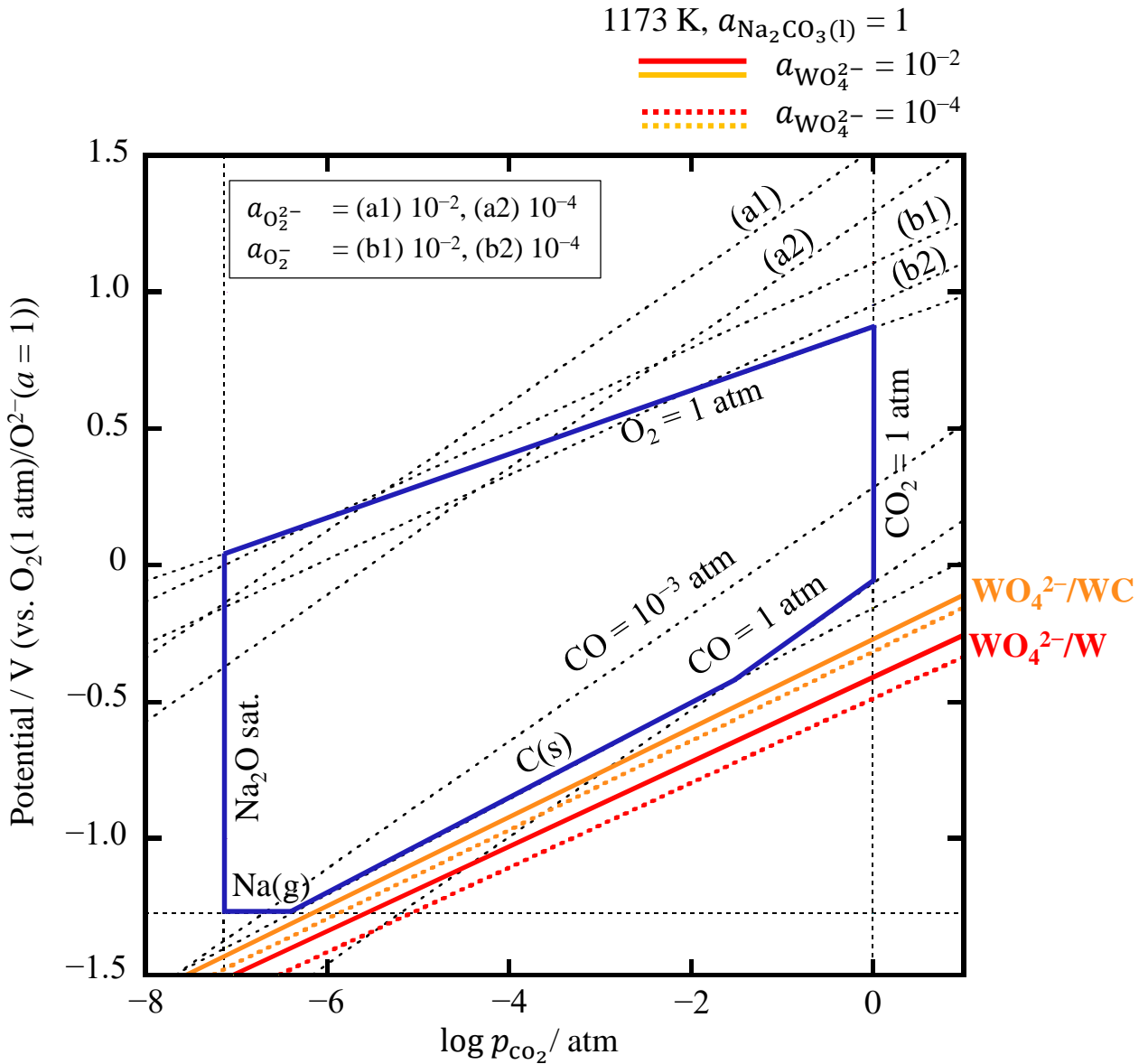


Figure 7 Calculated potential– $p_{\text{CO}_2}$  diagram from the reported thermodynamic data for W species (Red line) and WC species (Orange line) in molten  $\text{Na}_2\text{CO}_3$  at 1173 K from the reported thermodynamic data.<sup>31,32</sup> (Blue line) Stable region of molten  $\text{Na}_2\text{CO}_3$ . The solid and dotted color lines correspond to equilibria at the activity of  $\text{WO}_4^{2-}$  ion to be  $10^{-2}$  and  $10^{-4}$ , respectively.

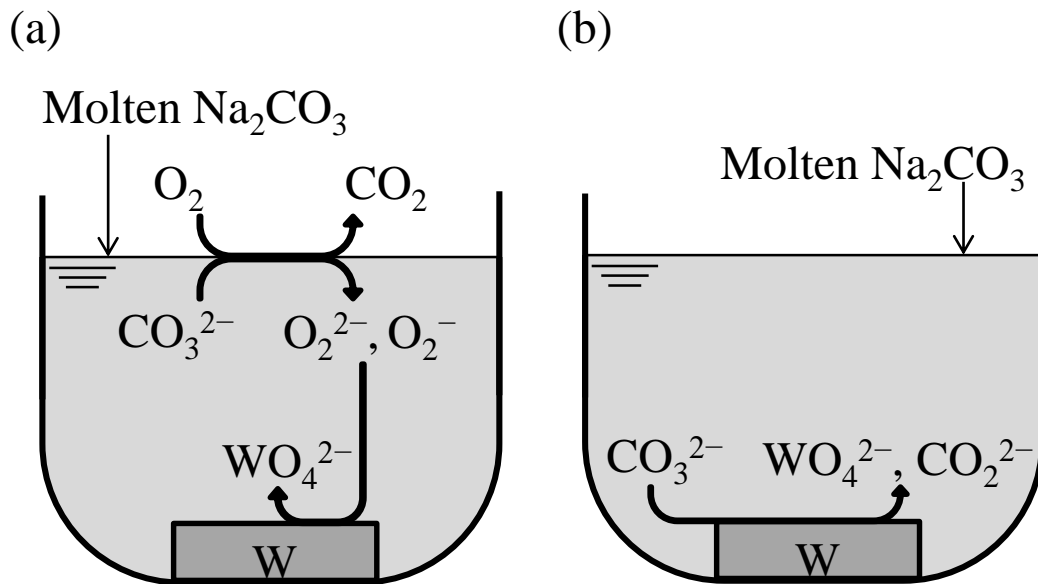


Figure 8 Schematic illustration of the reaction scheme of oxidative dissolution of tungsten metal in molten  $\text{Na}_2\text{CO}_3$  by (a)  $\text{O}_2^{2-}/\text{O}_2^-$  ions and (b)  $\text{CO}_3^{2-}$  ions

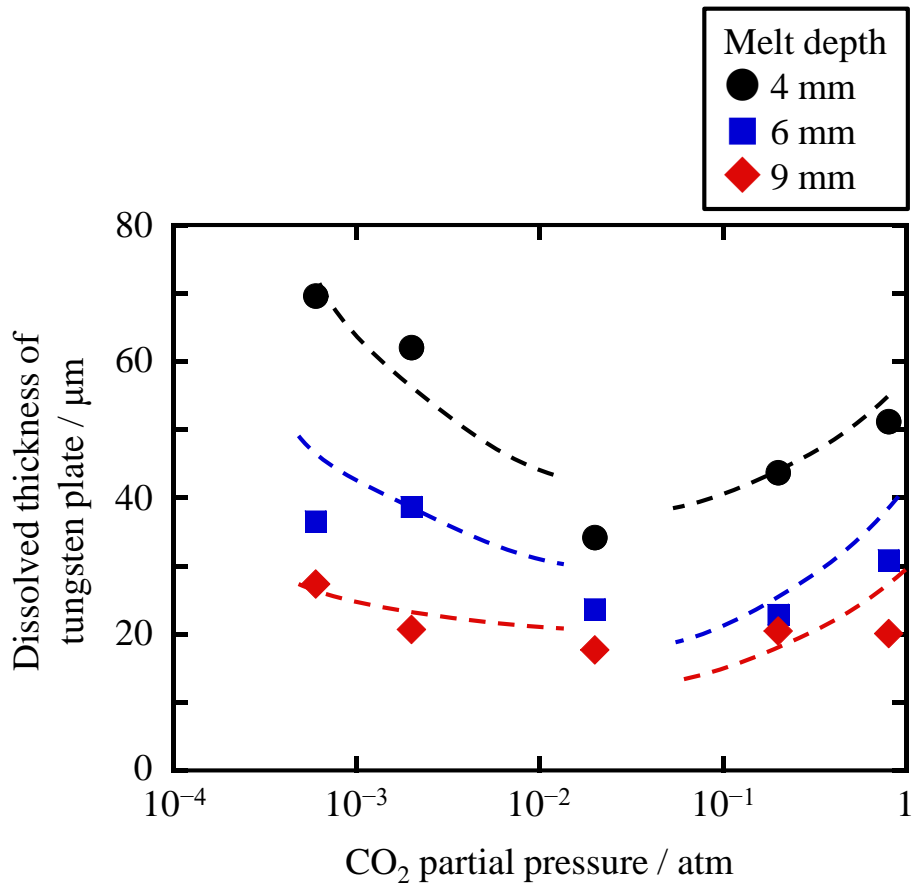
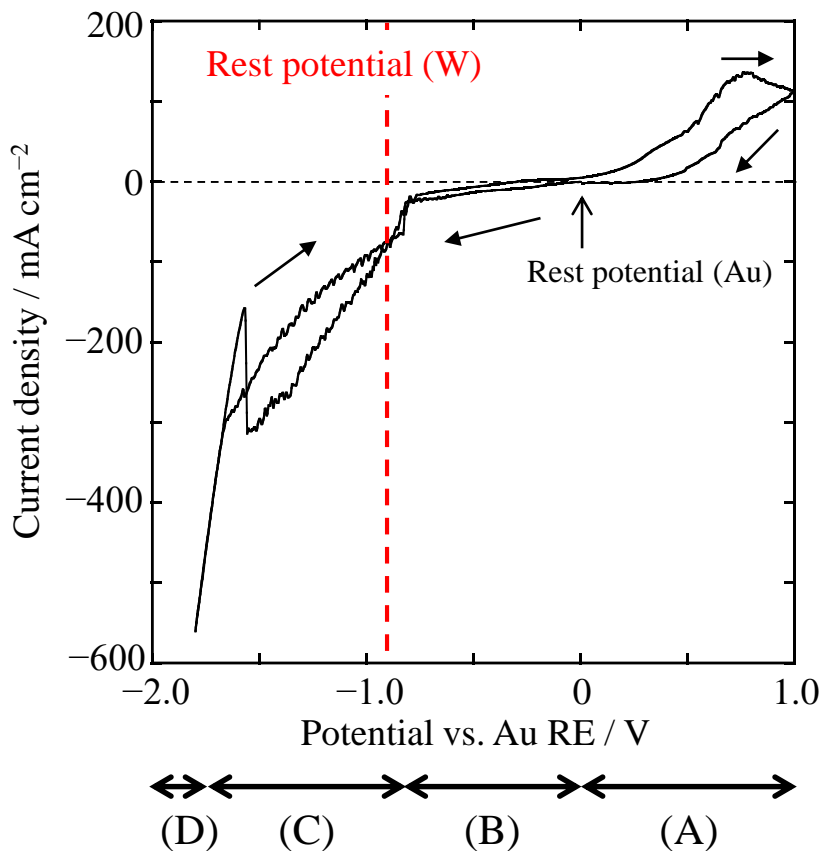


Figure 9 Dependence of dissolved thickness of tungsten plates on CO<sub>2</sub> partial pressure in molten Na<sub>2</sub>CO<sub>3</sub> at 1173 K in Ar-O<sub>2</sub>(0.2 atm)-CO<sub>2</sub> atmosphere for 2.5 h.



(b)

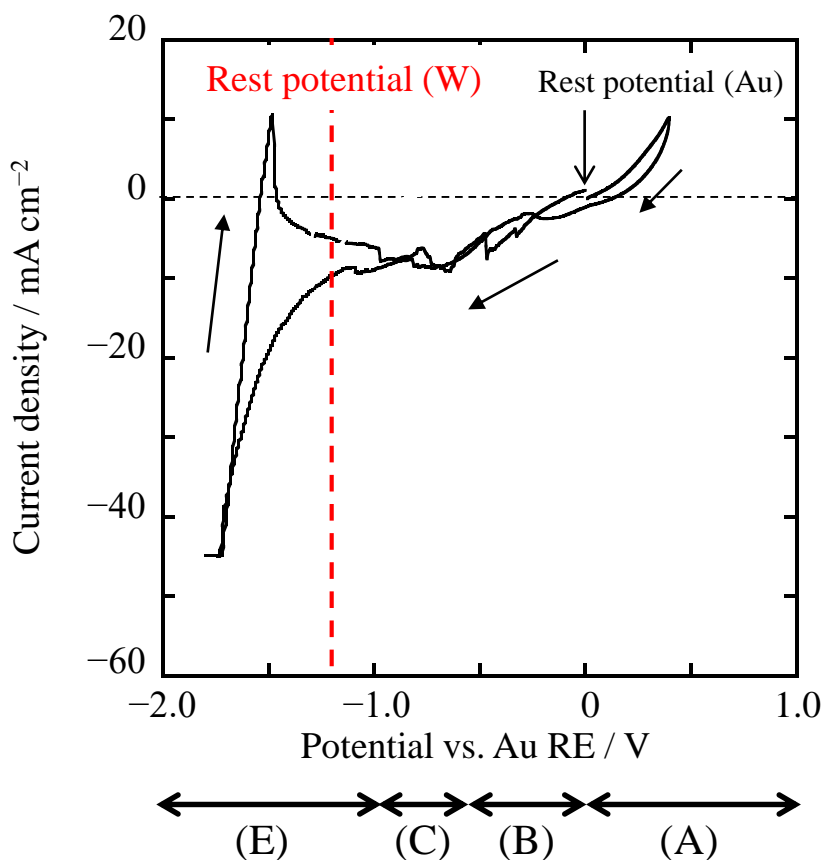


Figure 10 Cyclic voltammograms for Au wire electrode in (a) Ar–O<sub>2</sub>(0.2 atm)–CO<sub>2</sub>(6 × 10<sup>-4</sup> atm) and (b) O<sub>2</sub>(0.2 atm)–CO<sub>2</sub>(0.8 atm) in molten Na<sub>2</sub>CO<sub>3</sub> at 1173 K. Scan rate: 0.1 V s<sup>-1</sup>. (A) O<sub>2</sub> evolution, (B) O<sub>2</sub> reduction, (C) CO<sub>3</sub><sup>2-</sup> reduction, (D) Na gas evolution, and (E) C deposition.